Abrupt atmospheric torque changes and their role in the 1976-1977 climate regime shift

Steven L. Marcus, Olivier de Viron, Jean O. Dickey

Abrupt atmospheric torque changes and their role in the 1976–1977 climate regime shift

Steven L. Marcus,[1] Olivier de Viron,[2] and Jean O. Dickey[1]

Received 9 September 2010; revised 26 October 2010; accepted 3 December 2010; published 9 February 2011.

[1] During the climate regime/Pacific Decadal Oscillation (PDO) phase shift of 1976–1977, changes of up to several Hadleys occurred in the friction, mountain, and gravity wave torques that maintain the axial angular momentum (AAM) balance of the atmosphere. As required to produce a substantially different but stable climate regime, however, the total torque showed little net change (0.2 Hadley), while the AAM showed a modest increase, between the pretransition and posttransition periods in our data (1968–1975 and 1978–1997). The east-to-west transfer of atmospheric mass that occurs during the cold-to-warm phase shift of the PDO produced positive mountain torque anomalies on the atmosphere resulting from lower (higher) surface pressure to the west (east) of the Andes and Rockies (Himalayas), which were largely compensated by negative friction torque anomalies generated over the equatorial Pacific. The timing of events during the 1976–1977 transition window suggests that changes in low-latitude (Pacific friction and Andes mountains) torques and the PDO index in early to mid-1976 preceded changes in the extratropical torques during 1977, consistent with the poleward propagation of atmospheric zonal flow anomalies documented in previous studies. An increase in the global mean surface temperature and its rate of rise after the regime shift suggest that the negative friction torque anomalies that developed during the transition may have acted to sustain the warmer posttransition regime by suppressing cold-water upwelling in the eastern equatorial Pacific and/or equatorial thermocline heat content recharge processes in the central and western Pacific.

Citation: Marcus, S. L., O. de Viron, and J. O. Dickey (2011), Abrupt atmospheric torque changes and their role in the 1976–1977 climate regime shift, *J. Geophys. Res.*, *116*, D03107, doi:10.1029/2010JD015032.

1. Motivation and Methods

[2] The rate of global mean surface temperature (GMST) rise associated with anthropogenic forcing has not been constant but has shown considerable variability on decadal time scales during the past century. In particular, a slowdown in the rise of GMST during the middle of the twentieth century (approximately 1940–1975) and its subsequent speedup have drawn considerable attention, raising questions as to the possible role of internal climatic variability as well as changes in natural (e.g., volcanic) and anthropogenic (e.g., sulfate emission) forcing in fluctuations of global warming rates. The climate regime shift of 1976–1977 stands out as an archetypal example of such variability, and its causes and implications for future climate change continue to be the subject of ongoing research [e.g., *Meehl et al.*, 2009]. Here we investigate the processes that maintained the balance of atmospheric angular momentum (AAM) during the 1976–1977 regime shift and consider the possible role of associated torque changes in helping to define the altered heat balance of the warmer posttransition regime.

[3] The sharp nature of the transition has been noted by previous investigators [e.g., *Guilderson and Schrag*, 1998; *Frauenfeld et al.*, 2005], who highlighted the step-like change in equatorial Pacific sea surface temperature (SST) fields during the 1976–1977 regime shift. As an objective means of assessing the timing and strength of such transitions, we use the metric of variance explained (either fractional or absolute) by step functions fit to a given time series, as a function of the timing of the step. The time series consist of monthly mean data for atmospheric quantities over the period 1968–1997, with composite seasonal cycles removed; to gain a fuller perspective on the climate regime shift, global temperature data were examined back to 1957. Earlier atmospheric data were not used because of the lesser reliability of torque series before 1968 [e.g., *Weickmann et al.*, 2000], and data after 1997 were excluded to focus on the 1976–1977 regime shift, deferring consideration of additional regime changes that may have occurred in the post-1998 time frame to future work.

[4] The GMST data used in this study were taken from *Thompson et al.* [2009], who applied corrections for volcanic,

[1] Jet Propulsion Laboratory, California Institute of Technology, Pasadena, California, USA.
[2] University Paris Diderot and Institut de Physique du Globe de Paris, CNRS, Paris, France.

0148-0227/11/2010JD015032

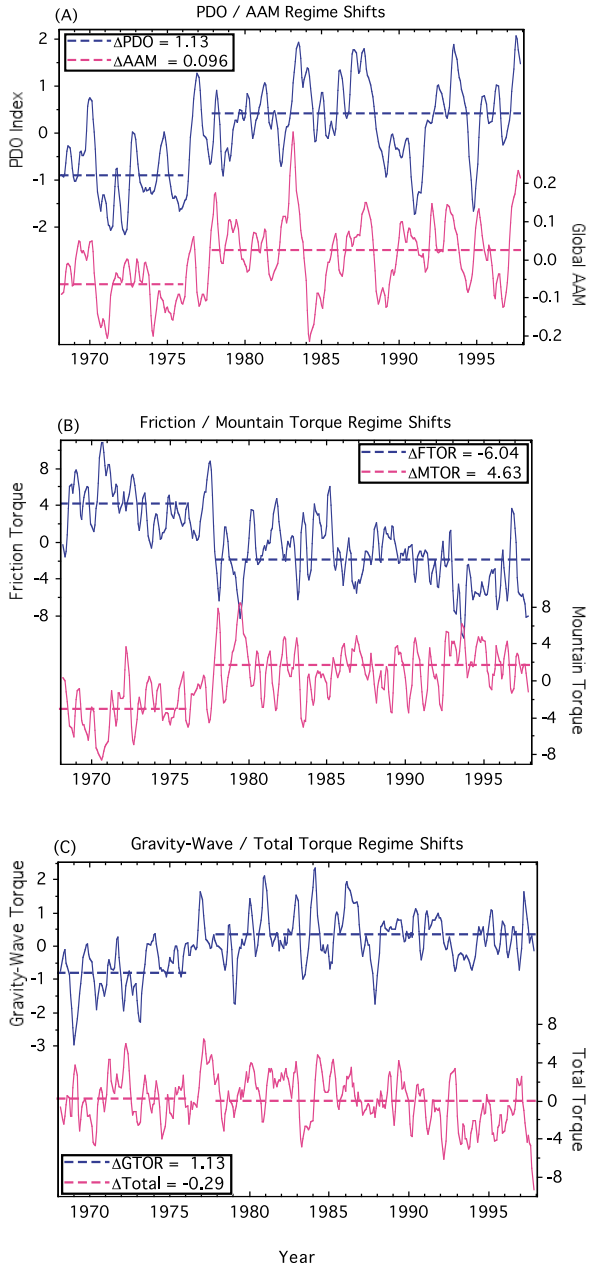

Figure 1. Time series plots showing 30 years (1968–1997) of monthly values with composite seasonal cycles removed and a 5 month running mean applied. The heavy dashed lines show mean values of each series for the pretransition and posttransition regimes, with the transition period (1976–1977) not included in the means. (a) PDO index (left axis) and global atmospheric angular momentum (right axis, 10^{26} kg m^2/s). (b) Friction torque (left axis, Hadleys = 10^{18} kg m^2/s^2) and mountain torque (right axis, with same vertical scale). (c) Gravity wave torque (left axis, on an expanded vertical scale) and total torque (right axis, on same vertical scale as Figure 1b).

dynamic, and El Niño–Southern Oscillation (ENSO) processes to surface temperature data sets provided by the Climate Research Unit at the University of East Anglia. We focus on the GMST series they derived from version 3 of the Hadley Centre Climate Research Unit combined land surface temperature and SST data set (HadCRUT3) [cf. *Brohan et al.*, 2006], using the corrections for volcanic and dynamic effects to study interannual variations in torque and surface temperature and removing the ENSO effects as well to study longer-term relationships between the two quantities.

[5] Atmospheric data were taken from the National Centers for Environmental Prediction/National Center for Atmospheric Research reanalysis [*Kalnay et al.*, 1996]. The context and mathematical expressions for computing the atmospheric torques in terms of surface stresses have been addressed in numerous papers [e.g., *Barnes et al.*, 1983; *Huang et al.*, 1999]. The axial torque is composed of three parts: a relatively small (for low frequency) gravity wave drag, which accounts for subgrid-scale interaction with the surface topography, and the friction and mountain torques, which are of the same order of magnitude. The gravity wave and friction torques can be computed directly from the corresponding drag (provided as output from the reanalysis models). The numerical calculation of the mountain torque can be complex, however, as it is a difference-like operation: The net torque acting over a mountain is the difference of the pressure action on the two sides. It can be computed from the scalar product (over the sphere) of the surface pressure and the longitudinal derivative of the topography, but this process is highly unstable, as the topography has strong variability on short-length scales. Better results are obtained by computing the scalar product of the surface pressure longitudinal derivative with the topography [cf. *Huang and Weickmann*, 2008], and this is the method adopted here.

2. Variations in the Global AAM Budget

[6] Evidence for regime-like behavior in the combined ocean-atmosphere system was first noticed in the North Pacific, where a pronounced deepening and eastward shift of the Aleutian Low, accompanied by wind-forced variations of SST in the central and eastern North Pacific, was found to have occurred during the winter of 1976–1977 [*Trenberth*, 1990]. Subsequent studies using models as well as observations [*Miller et al.*, 1994; *Trenberth and Hurrell*, 1994] found that extratropical SST variations could be accounted for by mixing, advection, and surface heat fluxes associated with local wind stress anomalies, which themselves appeared to be driven remotely by elevated SSTs in the central and eastern tropical Pacific [*Graham*, 1994]. These authors noted carefully that while exhibiting some of the characteristics of El Niño anomalies, the regime shift in the equatorial Pacific bore a closer resemblance to an increase in the temperature about which the oscillations occurred, rather than a change in the strength or period of the oscillations themselves.

[7] Subsequent investigators defined a new class of ocean-atmosphere variability, labeled the Pacific Decadal Oscillation (PDO), that seemed to capture the step-like decadal behavior found in the studies of the 1990s (Figure 1a, blue lines) [cf. *Mantua and Hare*, 2002]. Although defined by the first empirical orthogonal function of SSTs in the Pacific poleward of 20°N, the PDO spatial signature has been described as ENSO like [*Zhang et al.*, 1997], exhibiting like-signed SST anomalies in the central to eastern tropical Pacific and North American coastal waters surrounded by oppositely signed anomalies in the central extratropical and western

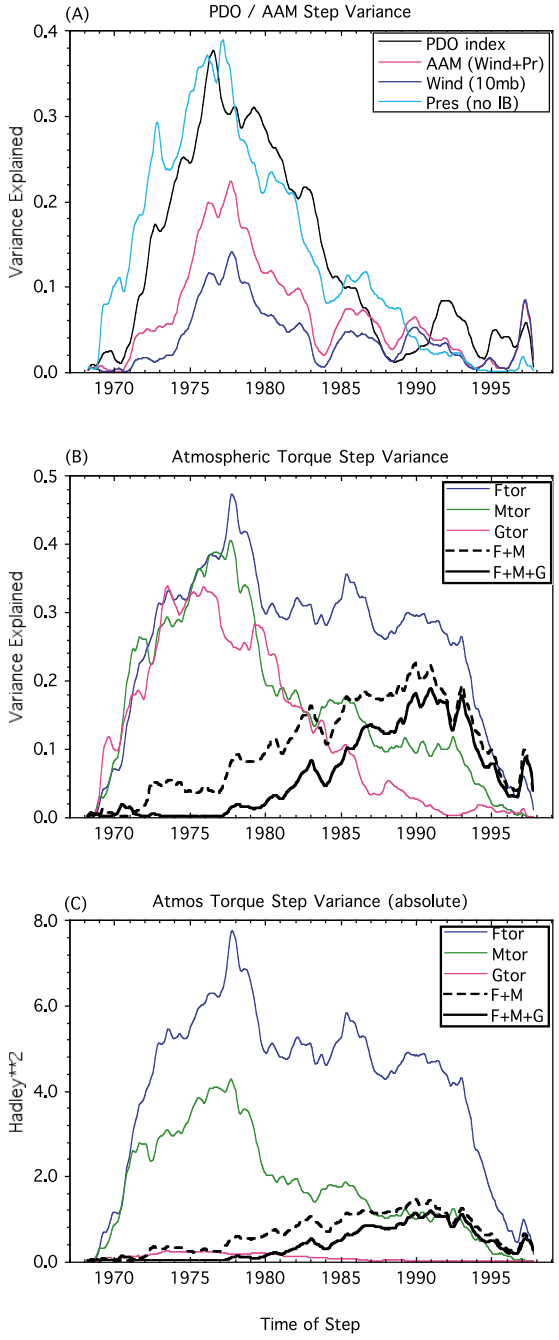

Figure 2. Variance explained in 30 year (1968–1997) monthly series with seasonal cycle removed and a 5 month running mean applied, by fitting step functions with arbitrary timing (bottom axis). (a) Fractional variances for the PDO index, global AAM, and its wind (integrated to 10 hPa) and pressure (computed without the inverted barometer assumption) components. (b) Fractional variances for the global friction, the mountain and gravity wave torques (colored lines), and the combined friction and mountain (black dashed line) and total (black solid line) torques. (c) As in Figure 2b but for the absolute variances.

tropical Pacific [*Shakun and Shaman*, 2009]; like ENSO, it also exhibits dynamical links to global-scale circulation anomalies [*Müller et al.*, 2008]. An important metric of the atmospheric circulation is given by its AAM, a dynamically conserved quantity whose generation by friction, mountain and gravity wave torques and transport via mean motion (meridional overturning circulations and standing waves), and transient eddies helps to define the Earth's current climate regime [*Egger et al.*, 2007]. The AAM (calculated from zonal winds integrated to 10 hPa and the non-inverted barometer pressure term [cf. *Zhou et al.*, 2006]) also shows clear evidence of a regime shift during 1976–1977 (Figure 1a, red lines), with its general similarity to the PDO indicating a possible causal relationship between them.

[8] The Earth-atmosphere torques that control the global AAM budget also show large changes during the regime shift; however, they tend to compensate each other so that the total torque changes very little on these time scales. Figure 1b, for example, shows that both the global friction and mountain torques undergo changes of several Hadleys during the same 1976–1977 time frame, but with opposite signs; similar opposite variations of the two torques on shorter time scales indicate the operation of a relatively rapid feedback between them [cf. *Weickmann et al.*, 2000]. Figure 1c (blue lines) shows that the gravity wave torque underwent a similar regime change at this time, although of lesser magnitude than the friction and mountain torques (note expanded vertical scale). Interestingly, the total torque (Figure 1c, red lines; here the vertical scale is the same as Figure 1b) shows virtually no shift, indicating that the regime changes in the individual torques adjusted to each other so that the total AAM was relatively constant before and after the transition (note that the AAM increase observed during the 1976–1977 regime shift corresponds to a net torque imbalance of only 0.2 Hadley, too small to be robustly identified from the existing torque series, acting over the 2 year transition period).

[9] To more quantitatively examine the regime behavior of these quantities, the variance explained by step functions in each series as a function of the timing of the step within the data record was computed. Figure 2a (black line) shows that the PDO index had a sharp break during 1976, with nearly 40% of its variance explained by a step function at that time, following removal of a composite seasonal cycle and application of a 5 month running mean. Interestingly, the AAM (Figure 2a, red line) shows a double peak in its step variance during the regime shift, with the first peak in early 1976 slightly preceding that seen for the PDO and a second, somewhat larger peak in late 1977. Similar timing is seen for the wind term of the AAM, which accounts for the bulk of the atmosphere's angular momentum variability. The pressure term, representing the smaller effect of changes in the atmosphere's axial moment of inertia, also has a double peak in its step-like behavior, of similar relative magnitude as the PDO.

[10] The relative variances explained by step functions in the global torques are shown in Figure 2b. The strongest step-like signal is seen in the friction torque in late 1977, similar in timing to the larger peak seen in the AAM step variance (Figure 2a). The mountain torque has a maximum at the same time but it is less pronounced, with relatively high values found during the full transition period (1976–1977). The gravity wave torque also shows its largest step variance

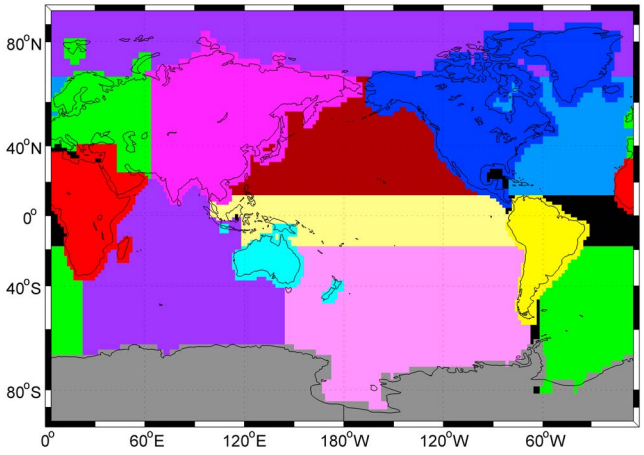

Figure 3. Geographical limits of the seven continental and eight oceanic areas used for the regional torque calculations.

about this time, with a broad maximum during the 1970s. It is interesting to note that the step variance found in the sum of the friction and mountain torques, represented by the black dashed line, shows relatively small values during the transition period, because of the efficient compensation between them; for the total torque (including gravity wave drag, shown by the heavy black line), the step-like behavior vanishes almost completely during this period. Thus it is accurate to describe the signature of the regime change in the angular momentum budget as a shift or exchange among the torque components, which mutually adjust to leave only a slowly changing total.

[11] Figure 2c shows the absolute variance explained by step functions in the torque series, in units of $(\text{Hadley})^2$. These curves are thus scaled versions of the relative variances shown in Figure 2b, with the friction torque having the largest step-like signature, the mountain torque having about half the step-function variance of the friction torque, and the gravity wave torque having much smaller values. The sum of friction and mountain torques (black dashed line) shows much less step variance; the full torque sum, including gravity wave effects (heavy black line), has a nearly vanishing step-like signature during the regime shift, again illustrating the efficient mutual adjustment among these torques to maintain the AAM balance.

3. Regional Mountain and Friction Torques

[12] The regional separation for the torque computations has been performed as follows. First, a different land-sea mask for the each quantity (i.e., friction or pressure torque) was used to define the continental and oceanic areas. Then longitude and latitude limits were used to apportion the ocean basins and continents to the regions shown in Figure 3, with the equatorial Atlantic and Pacific bounded by −15° and 15° of latitude. Mountain torques were then computed separately for each of the seven continents, and friction torques were computed for the same continental regions as well as the northern, equatorial, and southern Atlantic and Pacific oceans and for the Indian and Arctic oceans.

[13] Figure 4a shows the change in strength for the regional mountain torques, computed over the same time intervals as the global torques in section 2. The mountain torque changes are dominated by positive shifts originating over the three continents with major mountain ranges: Asia (Himalayas), South America (Andes), and North America (Rockies). Figure 4b shows the maximum fractional (absolute) variance explained in the time series for each region by a step change located within the 1976–1977 transition window, using black (red) symbols; those regions for which the 1976–1977 variance change was the largest for steps within the entire data interval (1968–1997) are shown in bold. As for the average change in the regional torques (Figure 4a), the fractional step variance (left axis) is largest for South America and Asia (approximately 20%), showing transitions, respectively, near the beginning of 1976 and 1977 (lower axis); for the other five regions the variance in the time series explained by steps within the 1976–1977 interval is at the 4% level or less. The absolute step variances for the different regions (right axis) are seen to be nearly proportional to the fractional variances, except for Asia, which shows a relatively high absolute variance because of its larger size and topography.

[14] Figure 4c shows the change in time-averaged strength for the regional friction torques during the regime shift. Unlike the mountain torques, which have comparable changes over three different areas of the globe, the friction torque changes are dominated by a single region, the equatorial Pacific. This torque is of particular interest since it may provide climate feedback by suppressing or enhancing cold upwelling along the South American coast and/or modifying recharge-discharge processes that affect heat storage in the equatorial thermocline layers of the Pacific on ENSO and decadal time scales [*Wang et al.*, 2003a, 2003b]. Figure 4d shows the timing and variance explained for step-function shifts located within the 1976–1977 transition window, for the friction torques computed separately over the seven continental (numbers) and eight oceanic (letters) regions; as for Figure 4b, areas where the variance explained in the window shown is a maximum for steps within the entire series are plotted in bold. The equatorial Pacific (region b) is seen to be dominant for the friction torque shift, both in terms of the fractional (black symbols, left axis) and absolute (red symbols, right axis) variance explained. The equatorial Atlantic also has a substantial fractional variance (region e); the north Atlantic and north Pacific (regions d and a, respectively) also have their largest changes during this window, although they are of smaller amplitude. Interestingly, these friction torque changes are seen to precede the mid-1976 PDO shift (Figure 4d, symbol p), which shows a fractional variance reduction intermediate in magnitude between that of the equatorial Pacific and Atlantic frictional torques.

[15] Figure 5 shows Hovmoeller (time-latitude) diagrams of the zonally averaged torques for the period of our study (1968–1997). The pre-1976 values of the mountain torque are characterized by strong negative anomalies at latitudes near 30°–50°N and 15°–30°S, corresponding to the highest elevations of the Himalayas and Rockies in the Northern Hemisphere (NH) and the Andes in the Southern Hemisphere (SH) (Figure 5, top). Following the 1976–1977 regime shift, the negative mountain torque anomalies in both hemispheres are sharply reduced in amplitude for the remainder of the study period, consistent with the positive torque shifts seen over Asia, South America, and North America at this time (Figure 4a), with changes at the latitude of the Andes

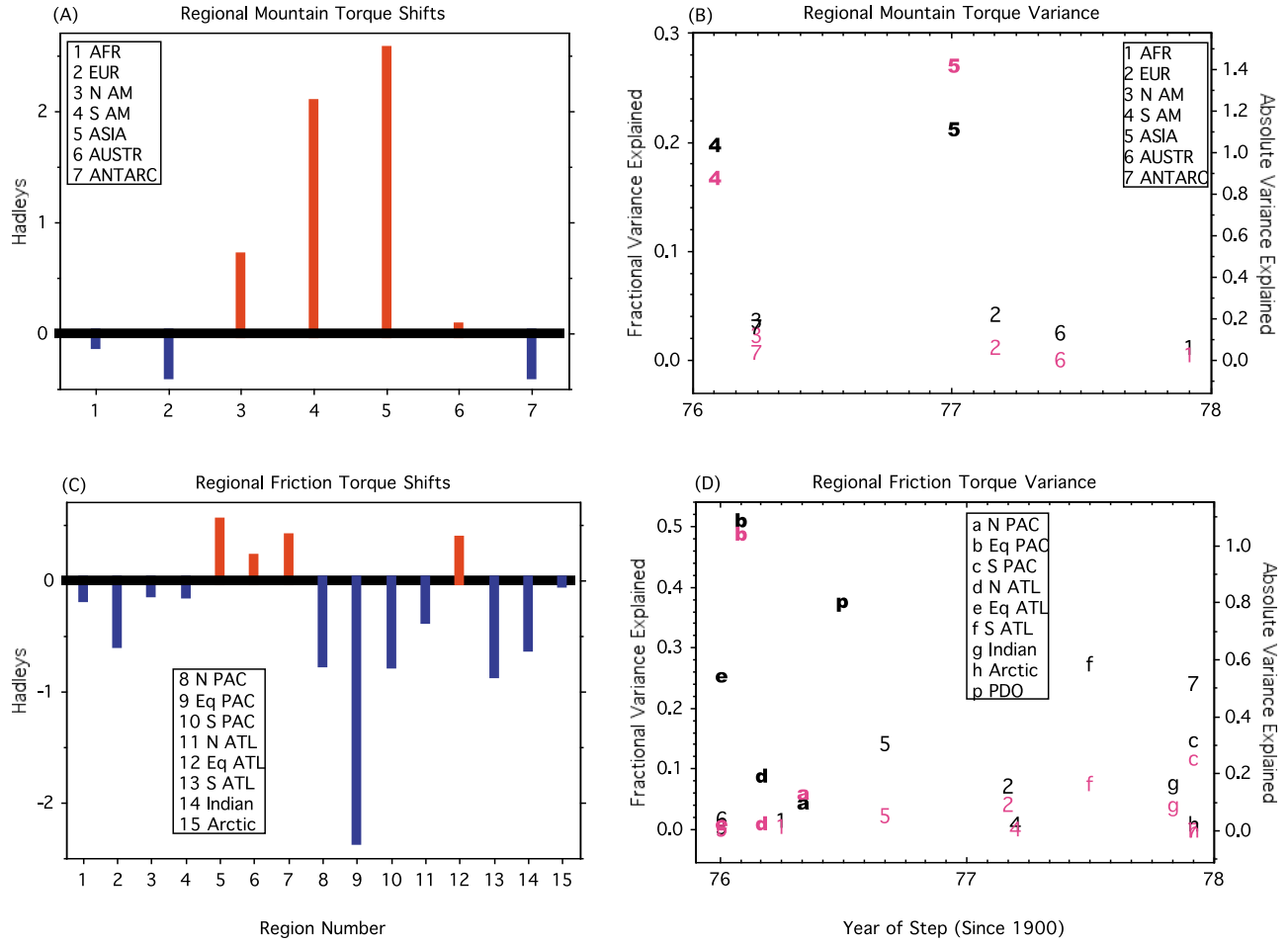

Figure 4. (a) Regional changes in mountain torques associated with the 1976–1977 regime shift, plotted as differences between the pre-1976 and post-1977 averages for the seven continental regions considered, using monthly time series spanning the period 1968–1997 with composite seasonal cycles removed and a 5 month running mean applied. (b) Maximum variances explained in the full (1968–1997) mountain torque time series by step changes positioned within the 1976–1977 interval (bottom axis); symbols show variances explained as a fraction of the total variance in each regional torque series (black, left axis) and absolute variances explained for each regional series in units of $(\text{Hadley})^2$ (red, right axis); for regions with bold symbols, the variance explained by steps within the 1976–1977 window is the maximum for steps within the entire period (1968–1997). (c) As in Figure 4a but for the friction torques, with eight oceanic regions added. (d) As in Figure 4b but for the friction torques, with the added oceanic regions and the PDO index denoted by letters.

preceding the higher-latitude torque changes in the NH. For the friction torque (Figure 5, middle), negative values become more prominent in both hemispheres after the 1976–1977 regime shift, with poleward propagation for anomalies of both signs clearly visible in the SH around this time. The total torque (Figure 5, bottom) shows a pattern of positive anomalies in the tropics flanked by negative anomalies in both hemispheres, which decreases in amplitude following the 1976–1977 regime shift; poleward propagation of the zonally averaged torque anomalies is visible in both hemispheres at this time, reaching subtropical latitudes in the NH and the extratropics in the SH.

[16] The latitude-longitude distribution of mountain and friction torque as well as surface pressure changes during the regime shift are shown in Figure 6. For the mountain torque (Figure 6, top), positive anomalies are seen for both the Andes and the Rockies. For the Himalayas, which generate strong mountain torques because of their large area and topography gradients, the signal is more mixed, as both positive and negative torque changes are seen; however, the net change is larger than that for the individual contributions from South and North America (although it is smaller than their sum; see Figure 4a). For the friction torque (Figure 6, middle), the clearest signal is seen over the eastern part of the tropical Pacific, consistent with the results presented in Figures 4c and 4d; note that the smaller values relative to the mountain torques are compensated by the larger area occupied by the friction torque anomalies. Interestingly, the negative torque anomalies are centered slightly off the equator in both hemispheres, where they may be particularly effective in exciting tropical recharge oscillations that affect the heat content of the equatorial Pacific thermocline layer [*Wang*

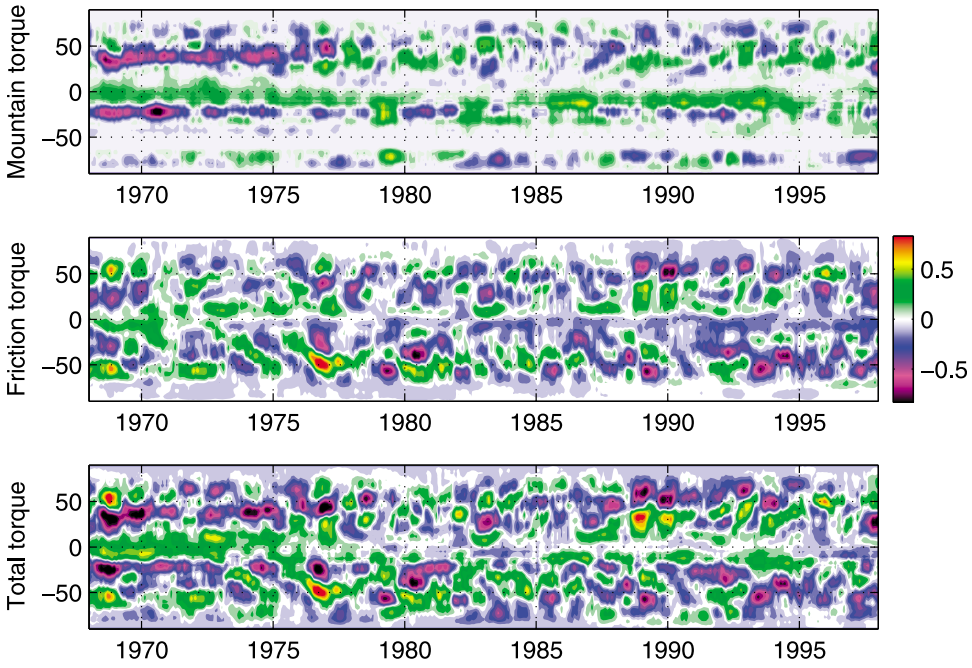

Figure 5. Hovmoeller (time-latitude) diagrams for the zonally averaged mountain torque and friction torque and their sum for the period of our study (1968–1997); warm (cold) colors denote eastward (westward) torque on the atmosphere (10^{18} Nm). Mountain torques (top) occur in two main belts near 40°N (20°S), corresponding to maximum elevations of the Himalayas and Rockies (Andes) in the northern (southern) hemisphere, with positive changes in the SH subtropics preceding those in the NH extratropics around the time of the 1976–1977 regime shift. Poleward propagation of the friction (middle) and total (bottom) torques is also visible in the SH at this time.

et al., 2003a, 2003b]. Finally, Figure 6c shows the surface pressure difference between the two regimes. Similar to the observed signal for the PDO [e.g., *Oshima and Tanimoto*, 2009], low (high) pressure anomalies are seen to the west (east) of the Rockies (Himalayas), generating positive mountain torque anomalies around the North Pacific (the effects of combined mountain torques from the Rockies and Himalayas on shorter time scales during boreal winter were previously noted [e.g., *White*, 1949; *Iskenderian and Salstein*, 1998]). An enhanced west–east pressure gradient is also seen over the steepest part of the Andes (15°–25°S), generating a net positive mountain torque adjacent to the South Pacific as well. Anomalous troughs also appear over the eastern subtropical Pacific in both hemispheres, leading to the off-equatorial surface westerlies that give rise to the negative friction torque anomalies seen in Figure 6b.

4. Climate Feedback Associated With Torque Changes

[17] Although the total atmospheric axial torque is relatively unaffected by the 1976–1977 regime shift (Figure 1c), its individual components undergo strong but compensating shifts during this time frame (Figure 4). Positive mountain torque changes caused by westward atmospheric mass transport in the Pacific basin, in particular, are compensated by negative friction torque changes, of which the largest (Figure 4c) and sharpest (Figure 4d) occurs over the equatorial Pacific (latitude 15°N–15°S). The role of frictional wind stresses in driving and providing feedback to tropical Pacific climate variability has long been known [e.g., *Bjerknes*, 1969], and the effects of this variability on global climate have also been recognized [e.g., *Thompson et al.*, 2009, and references therein]. To examine the possible role of the corresponding torques in providing feedback to the 1976–1977 climate regime shift, we compared changes in the GMST, corrected for volcanic and high-latitude land-ocean advection effects [cf. *Thompson et al.*, 2009], with time series of the equatorial Pacific friction torque with its sign reversed to give the atmospheric torque on the ocean, using yearly running means of both quantities. The correlation between the two detrended series (Figure 7a) shows significant maxima with positive values of the friction torque lagging the GMST by 10 months and with negative values of the friction torque (associated with anomalous surface westerlies) leading the GMST by 12 months.

[18] Time series of these two quantities with their trends restored are shown in Figure 7b; here the friction torque series has been lagged by 1 year and again reversed in sign (see right axis), with the relative scaling determined by linear regression of the GMST on the lagged friction torque during their period of overlap (1969–1997). A strong relationship is seen between interannual fluctuations in the two quantities as well as in their longer-term trends; note, in particular, that the step-like change in the friction torque during the 1976–1977 transition is mirrored by the GMST, although it is not until the 1980s that the temperature fully "catches up" with the larger (westerly) values of the torque. The negative correlation between the detrended friction torque and the GMST leading by 10 months appears to be nonphysical, since the series with

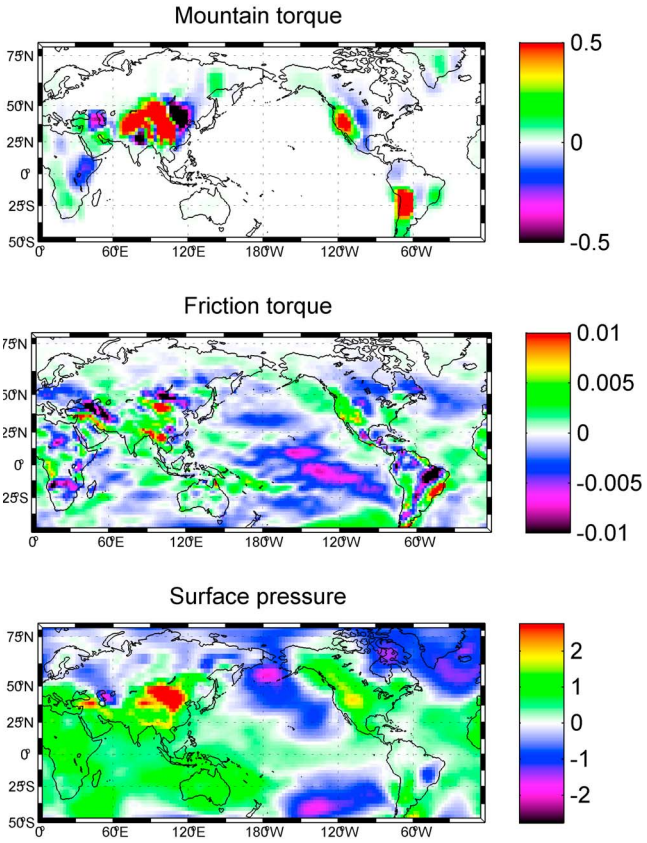

Figure 6. Regime shift changes, computed as the difference between averages over the periods 1968–1975 and 1978–1997. (top) Mountain torque (10^{18} Nm); note positive (eastward, warm color) anomalies over the Andes and Rockies and net positive anomalies over the Himalayas. (middle) As in Figure 6 (top) but for the friction torque; note pronounced negative (westward, cold color) anomalies located off-equator in both hemispheres of the eastern tropical Pacific. (bottom) Surface pressure (hPa); note positive (negative) anomalies in the west (east) subtropical and extratropical Pacific.

their trends restored have opposite slopes (data not shown). The robust correlation obtained with the GMST lagging suggests that the equatorial Pacific friction torque may influence temperatures on interannual (i.e., ENSO) time scales by suppressing upwelling in the East Pacific cold tongue [cf. *Neelin et al.*, 1998, and references therein] and may provide forcing on longer (decadal) time scales by influencing heat storage rates in the tropical Pacific through the recharge oscillator mechanism [*Wang et al.*, 2003a, 2003b], which can generate thermocline depth changes in the equatorial region that may act as an energy source or sink for the global ocean-atmosphere mixed layer.

[19] Some support for this view is provided by Figure 7c, which compares 5 year running mean values of the eastern equatorial Pacific friction torque (blue line, right axis) with centered, 10 year differences of the 5 year running mean GMST (red line, left axis); here the average rate of change of the GMST for the period considered (1.3°C per century) was added back into the temperature curve following linear regression of the GMST rate on the friction torque for display purposes. To focus on decadal time scales, ENSO effects were also removed from the GMST [*Thompson et al.*, 2009] for this comparison, and the frictional torque was computed using winds east of the dateline, where the regime shift anomalies (Figure 6, middle) and potential effects on decadal Pacific thermocline heat storage [*Wang et al.*, 2003a, 2003b] are strongest. The resemblance of the two curves suggests that friction torque over the eastern equatorial Pacific does exert an influence on GMST, which is independent of ENSO, or at least acts on longer time scales; interestingly, the detrended variations in the GMST rate and eastern equatorial Pacific friction torque show a closer relationship (Figure 7d), with a slightly higher correlation coefficient (0.95 versus 0.93 for the series with trends retained).

[20] A schematic of our findings is presented in Figure 8. The black lines show the GMST residuals for the 20 year periods 1957–1976 and 1978–1997 (left axis), as given by *Thompson et al.* [2009]. For the 20 years preceding the 1976–1977 regime shift, the GMST shows a slightly negative trend (dashed red line), indicating that the positive anthropogenic forcing during this time period [cf. *Hansen et al.*, 2007] was compensated by some source of natural variability or forcing other than the volcanic, advective, or ENSO effects removed by *Thompson et al.* [2009]. For the 20 years following the regime shift, the GMST residual shows a positive slope of 1.4°C per century (Figure 8, solid red line), suggesting that the compensating GMST forcing had ceased or reversed after the 1976–1977 transition. The dashed blue line shows the fractional variance explained by a step-function break within the 1968–1997 time series for the eastern equatorial Pacific friction torque; note that a remarkable 68% of the variance of the torque series can be explained by a step-function change at the time of the regime shift (1976), the largest for any quantity, global or regional, examined in this study.

[21] As discussed in previous sections of this study, the negative friction torques developing in the equatorial Pacific may be regarded as a dynamic consequence of the atmospheric mass shifts accompanying the cold-to-warm phase transition of the PDO, and the resulting positive mountain torques over the Himalayas, Andes, and Rockies. A region of weaker zonal pressure gradient change along the equator results in anomalous surface westerlies developing in two off-equator lobes (Figure 6, middle), where they can efficiently couple with the Pacific recharge oscillator on decadal time scales [*Wang et al.*, 2003b]. Thus it appears likely that the transformed (or, more precisely, redistributed) atmospheric torques arising during the regime shift may have helped to maintain the warmer posttransition climatic state by providing positive feedback to the altered thermodynamic balance of the Pacific equatorial thermocline.

5. Discussion and Conclusions

[22] The PDO bears many similarities to ENSO, as both involve warming of the equatorial eastern Pacific and a weakened Walker circulation [*Garcia and Kayano*, 2008], implying anomalous westerly surface winds in the tropical Pacific that may act to enhance the SST warming. While ENSO ocean-atmosphere anomalies are strongest in the equatorial waveguide, however, PDO anomalies have a broader latitudinal extent, with a particularly strong signature in the north Pacific (note the PDO index is defined as the first

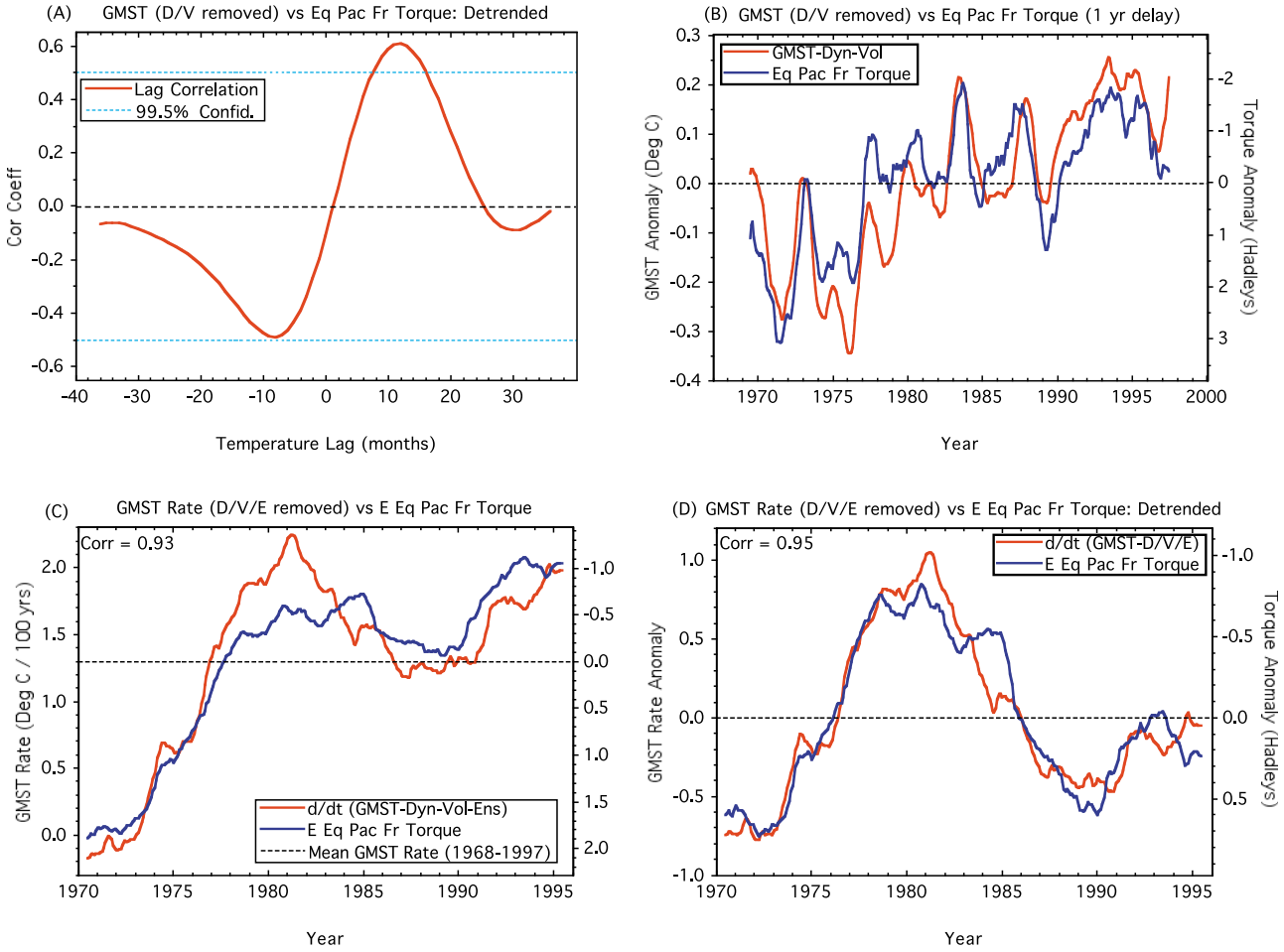

Figure 7. (a) Lag correlation coefficient between monthly time series of the GMST, corrected for dynamic and volcanic effects as described by *Thompson et al.* [2009], and equatorial Pacific friction torque (with sign reversed) for the period 1968–1997; annual mean smoothing and detrending were applied to both series. The largest correlations are obtained when the anomalous westerly friction torque on the equatorial Pacific leads the GMST by 12 months. (b) Time series of the GMST corrected for dynamical and volcanic effects (left axis) and equatorial Pacific friction torque (right axis; note reversed sign) with their trends restored. Annual smoothing was applied to both series, with the friction torque lagged by 12 months; the relative scaling between the left and right axes was determined by linear regression of the corrected GMST on the lagged torque. (c) Comparison of centered 10 year differences in the 5 year running mean GMST corrected for dynamic, volcanic, and ENSO effects (left axis), with the 5 year running mean equatorial Pacific friction torque computed east of the dateline (right axis), with the relative scaling between the axes determined by linear regression of the corrected GMST rate on the eastern equatorial Pacific friction torque. (d) As in Figure 7c but after first removing a linear trend from both series (note increased correlation coefficient).

empirical orthogonal function of SST north of 20°N). It also has a longer time scale (typically 20–30 years as opposed to 3–7 years for ENSO), and thus it may represent a reddened response of the ocean-atmosphere system to higher-frequency ENSO forcing [*Newman et al.*, 2003; *Shakun and Shaman*, 2009]. While a large body of theory and simulations with models of varying complexity have built up a considerable store of knowledge regarding the dynamical mechanisms that drive the ENSO cycle [cf. *Neelin et al.*, 1998, and references therein], the precise mechanisms that drive the PDO cycle have yet to be fully elucidated [e.g., *Stoner et al.*, 2009].

[23] While the physical mechanisms driving the PDO are unclear, however, the spatial anomalies associated with the PDO cycle have been well documented. This involves a coupled east–west variation of the ocean-atmosphere system across the Pacific basin, with the warm phase of the cycle characterized by lower (higher) atmospheric pressure over the east (west) Pacific, with the reverse behavior during the cool phase of the cycle. For the atmospheric angular momentum cycle, the relevant variables are the surface winds and the surface pressure changes over land, since these control the friction and mountain torques, respectively. As seen in Figure 6 (bottom), the warm phase involves an anomalous

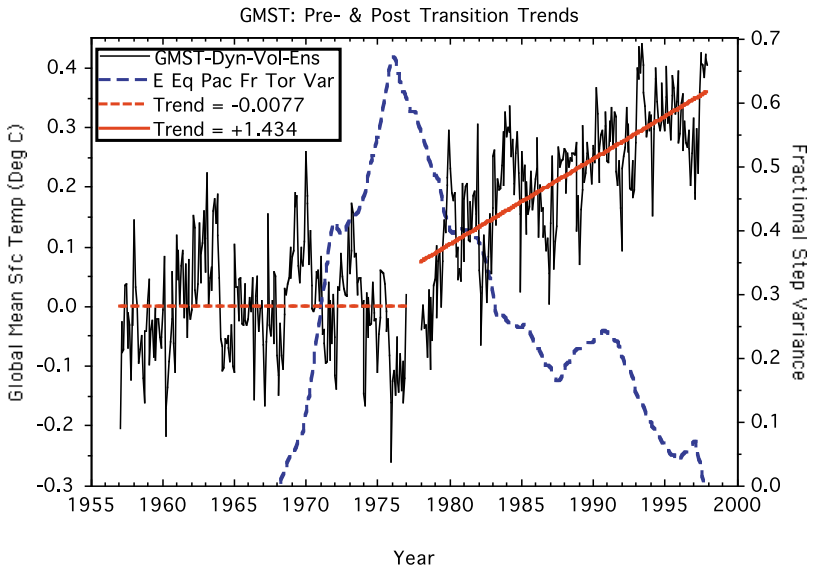

Figure 8. Global mean surface temperature (left axis) corrected for dynamic, volcanic, and ENSO effects [*Thompson et al.*, 2009] during the 20 years preceding (1957–1976) and following (1978–1997) the 1976–1977 climate regime shift, along with their unweighted least squares trend lines. Also shown is the fractional variance explained by step functions fit to the time series of eastern equatorial Pacific friction torque during the period 1968–1997 (right axis), with composite seasonal cycle removed and 5 month smoothing applied; note the large maximum for steps around 1976, coinciding with the sharp discontinuity in the rate of corrected GMST increase.

east–west surface pressure gradient over the subtropical and extratropical Pacific in both hemispheres, so that the resulting low (high) pressure anomalies to the west (east) of the Rockies and Andes (Himalayas) all produce positive shifts in the global mountain torque. The subtropical troughs in the eastern Pacific also produce anomalous off-equatorial surface westerlies in both hemispheres, giving rise to a major component of the negative friction torque that acts to balance the positive mountain torque anomalies associated with the positive phase of the PDO. As discussed in section 1, the mutual compensation between the substantial mountain, friction, and gravity wave torque changes results in a relatively constant net torque on the atmosphere, thus giving rise to a stable posttransition climate regime that differs substantially from the ocean-atmosphere state preceding the transition.

[24] The issue of causality was addressed by examining the timing of shifts in various quantities, using the metric of variance reduction by fitting to step functions. Changes in equatorial Pacific friction and South American mountain torques were found to occur first (early 1976), with the transition in the PDO index coming significantly later (mid-1976). Interestingly, changes in the largest mountain torque (Asia), and in the global torques, were seen to maximize later still (early and late 1977, respectively). The AAM step-like variance showed a double-peaked maximum, with the first (early 1976) coinciding with the initial torque changes in the equatorial Pacific and South America and the second coinciding with the timing of the total torque shift (late 1977). Thus the signatures of the regime change in the atmospheric angular momentum budget show some evidence of meridional evolution from equatorial to higher latitudes, similar to the poleward propagation of zonal flow anomalies discussed by *Dickey et al.* [1992, 2003] and *Lee et al.* [2007]. The initial causes of the torque and PDO index anomalies in 1976, however, remain to be determined.

[25] Since the strongest and sharpest of the negative friction torque shifts occurred over the equatorial Pacific, there is the potential for feedback from these torque changes on the posttransition climatic state. Time series of the equatorial Pacific friction torque, in particular, were found to lead changes in the GMST by about 1 year, with the latter corrected for volcanic and dynamic (land-ocean heat exchange) effects [cf. *Thompson et al.*, 2009]. The two series displayed an obvious correlation at interannual time scales, as well as similar trends over the time period studied (Figure 7b); however, the GMST response to the step-like change in the friction torque during 1976 was only fully realized in the 1980s, suggesting that the torque forcing may affect the longer-term (decadal) rate of change of the GMST as well as its shorter-term (interannual) fluctuations. This was found to be the case for the equatorial Pacific friction torque east of the dateline, for which the 5 year running mean bears considerable resemblance to centered 10 year differences of the 5 year running mean GMST (Figures 7c and 7d), with ENSO as well as dynamic and volcanic effects removed from the latter [cf. *Thompson et al.*, 2009].

[26] Our results suggest, therefore, that in addition to anthropogenic forcing [cf. *Meehl et al.*, 2009], the changes in atmospheric torques that accompanied the 1976–1977 regime shift (positive for mountain and gravity wave, negative for friction) helped to stabilize the warmer posttransition climate regime, by switching the Pacific decadal recharge oscillator to its discharge phase. The heat source thus provided to the global ocean-atmosphere surface layer is enough to account for a sizable portion of the GMST warming following the

1976–1977 regime shift, using thermocline temperature change estimates from ocean data assimilation models [cf. *Dewitte et al.*, 2009] and assuming that this energy is then "discharged" to the ocean-atmosphere surface layer (see Appendix A). Although the climate regime transition in 1976–1977 was quite sharp and well recognized in subsequent studies, indications of a reverse transition about 1998 are more ambiguous [e.g., *Bond et al.*, 2003; *Rodionov*, 2006]. A possible limiting factor to the warmer regime suggested by our work could be the depletion of the anomalous heat content of the Pacific thermocline layer, built up during the previous recharge phase of the oscillations described, for example, by *Wang et al.* [2003a, 2003b]. It should be noted, however, that the globally averaged heat fluxes associated with these oscillations are quite small compared to the planetary radiative imbalances arising from global warming [e.g., *Hansen et al.*, 2005]; thus the observed decadal variations in GMST rate, which may temporarily reinforce or cancel longer-term trends, should not be interpreted as altering the underlying reality of anthropogenic climate change.

Appendix A: Estimating the GMST Response to Thermocline Heat Discharge

[27] Following *Dewitte et al.* [2009], we assume a temperature decrease of 0.6°C over a depth range of 150 m averaged along the Pacific equatorial thermocline, following the 1976–1977 regime shift. Taking the horizontal dimensions of the cooling to be 120° longitude × 4° latitude, the total heat content change, averaged over the surface area of the Earth, is $\sim 4.4 \times 10^6$ J m^{-2}. *Thompson et al.* [2009], by comparing observed GMST changes with estimates of anomalous heat fluxes generated in the eastern equatorial Pacific, obtained an effective heat capacity for the ocean-atmosphere surface layer of 1.84×10^7 J m^{-2} K^{-1} for ENSO-related fluctuations, divided between an atmospheric component (1.0×10^7 J m^{-2} K^{-1}) and an oceanic component (0.84×10^7 J m^{-2} K^{-1}) equivalent to ~2 m average depth over the globe. Assuming that for PDO variations the atmospheric part of the heat capacity remains the same but that the depth of the affected oceanic layer scales with the square root of the period, and taking the respective ENSO and PDO recurrence times as 4 and 20 years, the effective ocean heat capacity becomes 1.9×10^7 J m^{-2} K^{-1}, giving a total surface layer heat capacity of 2.9×10^7 J m^{-2} K^{-1}. Thus, if we assume that an equivalent amount of heat is "discharged" from the Pacific equatorial thermocline to the ocean-atmosphere surface layer, the expected transient increase in GMST may be estimated as ~0.15°C.

[28] **Acknowledgments.** We thank David Thompson (Colorado State University) and colleagues for generously sharing their corrected global temperature data sets, Xiaochun Wang and Josh Willis of JPL for useful discussions of oceanic heat storage variations related to climate change, and two anonymous reviewers whose comments helped to improve the manuscript. This paper presents the results of one phase of research performed at the Jet Propulsion Laboratory, California Institute of Technology, sponsored by NASA. The contribution of O.d.V. to this study is IPGP contribution 3118.

References

Barnes, R. T. H., R. Hide, A. A. White, and C. A. Wilson (1983), Atmospheric angular momentum fluctuations, length-of-day changes and polar motion, *Proc. R. Soc. London, Ser. A*, *387*, 31–73, doi:10.1098/rspa.1983.0050.

Bjerknes, J. (1969), Atmospheric teleconnections from the equatorial Pacific, *Mon. Weather Rev.*, *97*, 163–172, doi:10.1175/1520-0493(1969)097<0163:ATFTEP>2.3.CO;2.

Bond, N. A., J. E. Overland, M. Spillane, and P. Stabeno (2003), Recent shifts in the state of the North Pacific, *Geophys. Res. Lett.*, *30*(23), 2183, doi:10.1029/2003GL018597.

Brohan, P., J. J. Kennedy, I. Harris, S. F. B. Tett, and P. D. Jones (2006), Uncertainty estimates in regional and global observed temperature changes: A new data set from 1850, *J. Geophys. Res.*, *111*, D12106, doi:10.1029/2005JD006548.

Dewitte, B., et al. (2009), Low-frequency variability of temperature in the vicinity of the equatorial Pacific thermocline in SODA: Role of equatorial wave dynamics and ENSO asymmetry, *J. Clim.*, *22*, 5783–5795, doi:10.1175/2009JCLI2764.1.

Dickey, J. O., S. L. Marcus, and R. Hide (1992), Global propagation of interannual fluctuations in atmospheric angular momentum, *Nature*, *357*, 484–488, doi:10.1038/357484a0.

Dickey, J. O., S. L. Marcus, and O. de Viron (2003), Coherent interannual and decadal variations in the atmosphere-ocean system, *Geophys. Res. Lett.*, *30*(11), 1573, doi:10.1029/2002GL016763.

Egger, J., K. Weickmann, and K.-P. Hoinka (2007), Angular momentum in the global atmospheric circulation, *Rev. Geophys.*, *45*, RG4007, doi:10.1029/2006RG000213.

Frauenfeld, O. W., R. E. Davis, and M. E. Mann (2005), A distinctly interdecadal signal of Pacific ocean-atmosphere interaction, *J. Clim.*, *18*, 1709–1718, doi:10.1175/JCLI3367.1.

Garcia, S. R., and M. T. Kayano (2008), Climatological aspects of the Hadley, Walker and monsoon circulations in two phases of the Pacific Decadal Oscillation, *Theor. Appl. Climatol.*, *19*, 117–127, doi:10.1007/s00704-007-0301-9.

Graham, N. E. (1994), Decadal-scale climate variability in the tropical and North Pacific during the 1970s and 1980s—Observations and model results, *Clim. Dyn.*, *10*, 135–162, doi:10.1007/BF00210626.

Guilderson, T. P., and D. P. Schrag (1998), Abrupt shift in subsurface temperatures in the tropical Pacific associated with changes in El Nino, *Science*, *281*, 240–243, doi:10.1126/science.281.5374.240.

Hansen, J., et al. (2005), Earth's energy imbalance: Confirmation and implications, *Science*, *308*, 1431–1435, doi:10.1126/science.1110252.

Hansen, J., et al. (2007), Climate simulations for 1880–2003 with GISS ModelE, *Clim. Dyn.*, *29*, 661–696, doi:10.1007/s00382-007-0255-8.

Huang, H. P., and K. M. Weickmann (2008), On the computation of the mountain torque from gridded global data sets, *Mon. Weather Rev.*, *136*, 4005–4009, doi:10.1175/2008MWR2359.1.

Huang, H. P., P. D. Sardeshmukh, and K. M. Weickmann (1999), The balance of global angular momentum in a long-term atmospheric data set, *J. Geophys. Res.*, *104*, 2031–2040, doi:10.1029/1998JD200068.

Iskenderian, H., and D. A. Salstein (1998), Regional sources of mountain torque variability and high-frequency fluctuations in atmospheric angular momentum, *Mon. Weather Rev.*, *126*, 1681–1694, doi:10.1175/1520-0493(1998)126<1681:RSOMTV>2.0.CO;2.

Kalnay, E., et al. (1996), The NCEP/NCAR 40-year reanalysis project, *Bull. Am. Meteorol. Soc.*, *77*, 437–471, doi:10.1175/1520-0477(1996)077<0437:TNYRP>2.0.CO;2.

Lee, S., S.-W. Son, K. Grise, and S. B. Feldstein (2007), A mechanism for the poleward propagation of zonal mean flow anomalies, *J. Atmos. Sci.*, *64*, 849–868, doi:10.1175/JAS3861.1.

Mantua, N. J., and S. R. Hare (2002), The Pacific decadal oscillation, *J. Oceanogr.*, *58*, 35–44, doi:10.1023/A:1015820616384.

Meehl, G. A., A. X. Hu, and B. D. Santer (2009), The mid-1970s climate shift in the Pacific and the relative roles of forced versus inherent decadal variability, *J. Clim.*, *22*, 780–792, doi:10.1175/2008JCLI2552.1.

Miller, A. J., D. R. Cayan, T. P. Barnett, N. E. Graham, and J. M. Oberhuber (1994), Interdecadal variability of the Pacific Ocean—Model response to observed heat-flux and wind stress anomalies, *Clim. Dyn.*, *9*, 287–302, doi:10.1007/BF00204744.

Müller, W. A., C. Frankignoul, and N. Chouaib (2008), Observed decadal tropical Pacific-North Atlantic teleconnections, *Geophys. Res. Lett.*, *35*, L24810, doi:10.1029/2008GL035901.

Neelin, J., D. S. Battisti, A. C. Hirst, F.-F. Jin, Y. Wakata, T. Yamagata, and S. E. Zebiak (1998), ENSO theory, *J. Geophys. Res.*, *103*, 14,261–14,290, doi:10.1029/97JC03424.

Newman, M., G. P. Compo, and M. A. Alexander (2003), ENSO-forced variability of the Pacific decadal oscillation, *J. Clim.*, *16*, 3853–3857, doi:10.1175/1520-0442(2003)016<3853:EVOTPD>2.0.CO;2.

Oshima, K., and Y. Tanimoto (2009), An evaluation of the reproducibility of the Pacific Decadal Oscillation in the CMIP3 simulations, *J. Meteorol. Soc. Jpn.*, *87*, 755–770, doi:10.2151/jmsj.87.755.

Rodionov, S. N. (2006), Use of prewhitening in climate regime shift detection, *Geophys. Res. Lett.*, *33*, L12707, doi:10.1029/2006GL025904.

Shakun, J. D., and J. Shaman (2009), Tropical origins of North and South Pacific decadal variability, *Geophys. Res. Lett.*, *36*, L19711, doi:10.1029/2009GL040313.

Stoner, A. M. K., K. Hayhoe, and D. J. Wuebbles (2009), Assessing general circulation model simulations of atmospheric teleconnection patterns, *J. Clim.*, *22*, 4348–4372, doi:10.1175/2009JCLI2577.1.

Thompson, D. W. J., J. M. Wallace, P. D. Jones, and J. J. Kennedy (2009), Identifying signatures of natural climate variability in time series of global mean surface temperature: Methodology and insights, *J. Clim.*, *22*, 6120–6141, doi:10.1175/2009JCLI3089.1.

Trenberth, K. E. (1990), Recent observed interdecadal climate changes in the Northern Hemisphere, *Bull. Am. Meteorol. Soc.*, *71*, 988–993, doi:10.1175/1520-0477(1990)071<0988:ROICCI>2.0.CO;2.

Trenberth, K. E., and J. W. Hurrell (1994), Decadal atmosphere-ocean variations in the Pacific, *Clim. Dyn.*, *9*, 303–319, doi:10.1007/BF00204745.

Wang, X. C., F. F. Jin, and Y. Q. Wang (2003a), A tropical recharge mechanism for climate variability: part I. Equatorial heat content changes induced by the off-equatorial wind, *J. Clim.*, *16*, 3585–3598, doi:10.1175/1520-0442(2003)016<3585:ATORMF>2.0.CO;2.

Wang, X. C., F. F. Jin, and Y. Q. Wang (2003b), A tropical ocean recharge mechanism for climate variability: part II. A unified theory for decadal and ENSO modes, *J. Clim.*, *16*, 3599–3616, doi:10.1175/1520-0442(2003)016<3599:ATORMF>2.0.CO;2.

Weickmann, K. M., W. A. Robinson, and C. Penland (2000), Stochastic and oscillatory forcing of global atmospheric angular momentum, *J. Geophys. Res.*, *105*, 15,543–15,557, doi:10.1029/2000JD900198.

White, R. M. (1949), The role of mountains in the angular momentum balance of the atmosphere, *J. Meteorol.*, *6*, 353–355.

Zhang, Y., J. M. Wallace, and D. S. Battisti (1997), ENSO-like interdecadal variability 1900–93, *J. Clim.*, *10*, 1004–1020, doi:10.1175/1520-0442(1997)010<1004:ELIV>2.0.CO;2.

Zhou, Y. H., D. A. Salstein, and J. L. Chen (2006), Revised atmospheric excitation function series related to Earth's variable rotation under consideration of surface topography, *J. Geophys. Res.*, *111*, D12108, doi:10.1029/2005JD006608.

J. O. Dickey and S. L. Marcus, Jet Propulsion Laboratory, California Institute of Technology, Mail Stop 238-600, 4800 Oak Grove Dr., Pasadena, CA 91109, USA. (steven.marcus@jpl.nasa.gov)

O. de Viron, University Paris Diderot and Institut de Physique du Globe de Paris, CNRS, Paris 75005, France.